Wind-Driven Motions in the Northeast Pacific as Measured by Lagrangian Drifters

PEARN P. NIILER

Scripps Institution of Oceanography, University of California, San Diego, La Jolla, California

JEFFREY D. PADUAN

Department of Oceanography, Naval Postgraduate School, Monterey, California

(Manuscript received 21 September 1994, in final form 20 January 1995)

ABSTRACT

Analysis is presented of the time-dependent motion of 47 surface drifters in the northeast Pacific during fall 1987 and 16 drifters in fall and winter 1989/90. The drifters were drogued at 15-m depth and were designed to have wind-produced slips less than 2 cm s^{-1} for wind speeds up to 20 m s^{-1}. The coherence of velocity and local wind is presented for motions with periods between 1 day and 40 days. For periods between 5 and 20 days, drogue motion at 15-m depth is found to be highly coherent with local wind with an average phase of 70° to the right of the rotating wind vector. These results differ from analyses of FGGE-type drifters as reported by McNally et al. and Niiler in the same area. A model of wind-produced slip as a function of drifter design is used to provide a possible explanation of the differences. A linear regression, which accounts for 20%–40% of the current variance, gives water motion at 0.5% of wind speed and 68° to the right of the wind vector. Assuming an Ekman-type balance, this regression with 15-m currents yields an apparent mixing depth of 34–38 m, which is much less than the observed 60-m depth of the mixed layer. New three-parameter models for turbulent stress are presented based on these observed depth scales and regression coefficients. The model stresses rotate from downwind to crosswind at the base of the mixed layer. The model currents rotate from approximately 60° to the right of the wind vector at the surface to 180° to the right of the wind vector at the mixed layer base.

1. Introduction

In the northeast Pacific, two very different pictures have emerged of the relationship of mixed layer currents to surface winds from current meter measurements and drifting buoys. Davis et al. (1981) describe measurements from strings of current meters moored beneath surface buoys and show that wind-coherent, subinertial currents below 5-m depth are 60°–100° to the right of the surface wind stress for periods of 1–4 days. In contrast, McNally (1981), Niiler (1986), and McNally et al. (1989), who analyzed motion of FGGE-type drifters, show that mixed layer currents with periods of 3–30 days, as determined by these drifters, are less than 30° to the right of the surface wind stress. A FGGE-type (or McNally-type) drifter typically has a 2-m long, 10-cm diameter metal or fiberglass surface float with a mass between 100 and 250 kg, to which a window-shade or parachute drogue is attached at 30-m depth. Because several observers (Kirwan et al. 1978; McNally and White 1985) found no difference in FGGE drifter motion with the drogue indicator showing attached drogue or showing lost drogue, the analysis has been done with the firm belief that the FGGE surface float motion actually represents the motion of water. These differences in wind-driven current direction and amplitude between current meter data and FGGE-type drifters are significant, especially when studying the effects of circulation on the horizontal transport of heat, salt, and other constituents. In this paper we present a possible resolution of the discrepancy by analyzing motion of a set of newly designed Lagrangian drifters in the northeast Pacific.

The water-following capability of any mixed layer drifter depends critically upon the drag area ratio R, which is the ratio of the product of the drag coefficient of the drogue and its frontal area to the sum of the products of the drag coefficients and frontal areas of the fully submerged floats and tether. The drag area ratio for our instruments ranged from 50 to 70. FGGE drifters with window shade drogues have a drag area ratio of 10–12. McNally's drifters, with a fully flooded parachute, would have a drag area ratio comparable to the drifters that we use here. However, the moment that a parachute closely follows the water it may be expected to collapse and not open again. McNally's drifters, therefore, may have had operational drag area ratios even smaller than FGGE-type drifters with win-

Corresponding author address: Dr. Jeffrey D. Paduan, Department of Oceanography, Code OC/Pd, Naval Postgraduate School, Monterey, CA 93943.
E-mail: paduan@nps.navy.mil

dow-shade drogues. It is impossible to verify the behavior of these instruments without extensive in-water calibration studies. We note, however, that results based on undrogued FGGE-type surface floats (e.g., Niiler 1986) are similar to those based on McNally-type instruments with drogues of unknown effectiveness. Our objective here in comparing our results with those of earlier drifter studies is simply to point out that observed differences in wind-driven currents may reasonably be described by differences in the water-following capabilities of the different instruments without invoking any differences in ocean physics or conditions between the various study years.

As part of the OCEAN STORMS Experiment in October 1987, we deployed 47 mixed layer drifters in the vicinity of 47°N, 140°W. In October 1989, we deployed 16 additional mixed layer drifters as part of the WOCE Heavy Weather Test. Each drifter had a three-dimensional, rigid-frame cloth drogue tethered at 15-m depth and a surface float consisting of a 30-cm diameter fiberglass sphere (Niiler et al. 1987; Sybrandy and Niiler 1991). The drifters we used have also been subjected to in situ calibrations of the effect of winds on drifter motion by attaching VMCMs directly to their drogues (Niiler et al. 1987; Niiler et al. 1995). Our general result is that, while wind-driven motions are very difficult to measure in the presence of mesoscale activity—even in this supposed "eddy desert"—the analysis we present shows that the drogue motion is between 65° and 85° to the right of surface wind (or wind stress). This result is consistent with moored measurements and further indicates that FGGE-type drifters have a significant slip in the direction of wind. Using the statistical model of drogue slippage as a function of wind speed and drag area ratio developed by Niiler et al. (1995), we show that drifters with drag area ratios in the range of FGGE drifters are expected to travel at less than 30° to the right of the surface wind (the appendix) and, therefore, they are not good markers of ocean surface currents.

Finally, our analysis suggests that there is significant rotation of the vertical turbulent stress gradient (i.e., currents) through the mixed layer. In a mixed layer model where the velocity is independent of depth, the stress gradient is always 90° to the right of the surface velocity. We present two simple alternative models for turbulent stress profiles in a mixed layer and discuss the rotating velocity field associated with them as a function of the depth scales of the mixed layer and the turbulent convergence measured at the drogue depth of 15 m. The implied rotation of the mixed layer velocity is presented for the parameters determined by our observations. These indicate that the surface current is approximately 60° to the right of the surface stress and the current at the base of the mixed layer is approximately 180° to the right of the surface stress.

This paper is organized as follows. In section 2 we describe the surface drifter and wind datasets. In section 3 we present the statistical results of comparing vector winds and currents, including sample quadratic and exponential formulations for stress in the upper ocean. A simple theoretical model that shows the current response of a mixed layer drifter to be a predictable function of its drag area ratio is presented in the appendix, and all results are summarized in section 4.

2. The data

The first velocity database for this work derives from ARGOS position returns from 47 TRISTAR-II drifters deployed during the OCEAN STORMS Experiment in the northeast Pacific in October of 1987. This dataset has been described by Paduan and Niiler (1993) in terms of its subinertial velocity statistics and heat advection implications for the three-month, fall period of October–December 1987. The trajectories from all drifters are shown in Fig. 1a, where the individual position time series have been low-passed filtered to remove inertial currents using a cosine filter with a half-power point of 96 hours. The instruments themselves have been described by Niiler et al. (1987) and consist of a large three-axis symmetric drogue in the shape of a radar reflector centered at 15 m. Most importantly, the instruments have been calibrated for slippage as a function of wind speed, drag area ratio, and velocity shear across the drogue (Niiler et al. 1987; Niiler et al. 1995). The drogue is supported by small, spherical surface and subsurface floats containing an ARGOS transmitter, batteries, and antenna. These instruments have drag area ratios of approximately 70, for which the slip of the drogue through the water is less than 2 cm s^{-1} for wind speeds less than 20 m s^{-1}. All of the OCEAN STORMS drifter data used in this study come from observations where the drogues were firmly attached as evidenced by subsurface temperature data from along the tether line (Paduan and Niiler 1993).

The second velocity database derives from the ARGOS position returns from 8 Holey-sock drifters and 8 MINISTAR (a smaller version of the TRISTAR) drifters deployed during the WOCE Heavy Weather Drifter Test in the northeast Pacific from October 1989 through April 1990. These data were low-pass filtered using a butterworth filter with a half-power point of four inertial periods, or about 65 hours. The trajectories of all 16 drifters are shown on Fig. 1b. The Holey-sock instruments themselves have been described by Sybrandy and Niiler (1991) and consist of 1-m diameter by 6.5-m long Holey-sock drogue and spherical flotations. The drag area ratio of the Heavy Weather drifters was 50.

The wind data used to compare with drifter-derived currents from the 1987 and 1989/90 datasets came from 6-hourly surface winds derived from the operational weather product of the European Centre for Medium-Range Weather Forecasts (ECMWF), which were interpolated onto 6-hourly filtered drifter positions. In cases where wind stresses were used in the

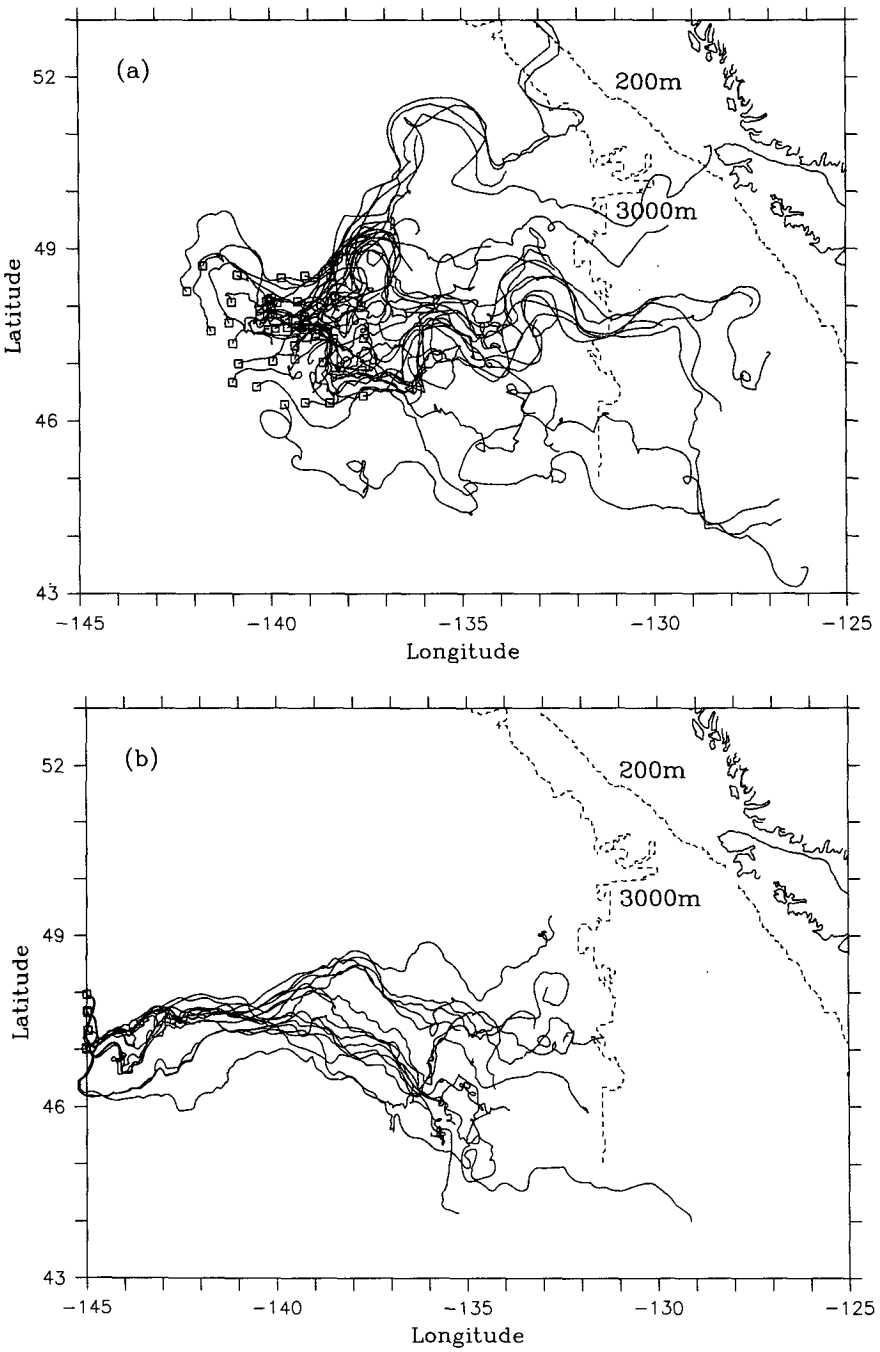

FIG. 1. Trajectories of TRISTAR-II drifters in the (a) OCEAN STORMS Experiment for the period Oct–Dec 1987 and (b) MINISTAR and Holey-Sock drifters in the WOCE Heavy Weather Test for the period Oct 1989–Apr 1990. Deployment locations are denoted by the square symbols.

analyses, they were computed using a constant, neutral drag coefficient of 1.2×10^{-3}. The basic data used in these analyses was, therefore, wind (or wind stress) and drifter-derived currents at the location of each drifting buoy as a function of time. Based on analysis of drogue slippage as a function of wind speed, the drifters used in 1987 are known to exhibit a downwind slip of 0.05 cm s^{-1} per m s^{-1} of wind speed. The drifters used in 1989/90 exhibit a downwind slip closer to 0.07 cm s^{-1} per m s^{-1} of wind speed. These corrections have been applied to all the velocity data used in these analyses. We chose ECMWF winds after we compared

that product with buoy, mooring, and ship wind measurements in the OCEAN STORMS area for the period of October–December 1987. We found no biases in wind direction between the standard ECMWF product and the local wind observations.

3. Relationship of drifter motion to wind stress

a. Surface current and wind coherence

A cross-spectral analysis between drifter-derived currents and wind stress can be used to test the coherence and phase relationships of the two time series as a function of frequency. In particular, the phase results within the low-frequency band can be compared with the value of −90°, which indicates water motion at 90° to the right of the rotating wind vector, given an idealized mixed layer where velocity is independent of depth. McNally et al. (1989) employed this statistical analysis on their FGGE-type drifter data and winds derived from the Fleet Numerical Oceanographic Center (FNOC) analyses. They found subinertial current motions at less than 30° to the right of the wind vector. They used FNOC wind products because independent measurements with moored buoys during NORPAX showed that to be an excellent product for the northeast Pacific Ocean (Pazan and Friehe 1978). At that time, ECMWF winds had not been as extensively verified in this region.

In this study, the complex rotary spectrum and cross spectrum were computed for each drifter time series longer than 40 days. Each 40-day drifter segment and its accompanying wind stress segment were used to produce rotary spectral estimates of drifter-derived velocity and wind stress. The combined vector current and wind stress segments were used to produce estimates of coherence squared and phase in the 1 to 40 day band. The 1987 OCEAN STORMS drifter and wind stress data provided 66 ensembles of 40-day length. The 1989/90 Heavy Weather data provided 67 ensembles of 40-day length. The rotary spectra and cross-spectra were ensemble averaged and then band averaged for each of the 1987 and 1989/90 datasets. The average rotary spectra for drifter-derived velocity and wind stress during the OCEAN STORMS and Heavy Weather Experiment periods are presented in Figs. 2a and 2b. In both datasets, the wind stress spectra are relatively flat across the frequency range compared with the velocity spectra. There is evidence for slightly higher clockwise energy than counterclockwise energy in both velocity and wind stress in both datasets. The Heavy Weather drifter velocity data show a strong roll-off for periods shorter than 3 days in the velocity spectra, which reflects the different filtering applied to that dataset compared with the OCEAN STORMS drifter data rather than real differences in the current properties at higher frequencies. Finally, an unexplained but significant difference in the counterclockwise energy at

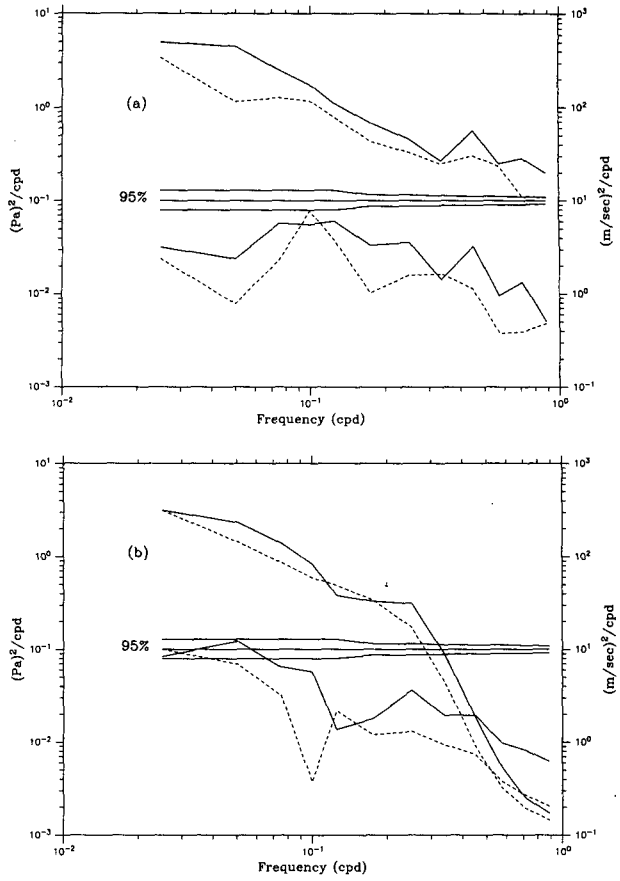

FIG. 2. Rotary spectra for the clockwise-rotating (solid) and counterclockwise-rotating (dashed) velocity (upper pair, right axis) and wind stress (lower pair, left axis) from the OCEAN STORMS (a) and Heavy Weather Experiment (b) drifter velocity and ECMWF wind stress data. Velocity data was corrected for wind slip prior to computation of the spectral estimates. Forty-day segments were ensemble averaged and then band averaged to obtain the averaged spectra. The 95% confidence limits for the equivalent one-sided autospectra are presented for reference.

10-day periods exists between the ECMWF data for the OCEAN STORMS period and the Heavy Weather period. The former contains a relative peak at that frequency, whereas the latter contains a relative trough at that frequency. This slightly anomalous behavior at the 10-day period for counterclockwise wind motions is reflected in the cross-spectral results presented below but, otherwise, the spectral results are fairly uniform across the band of frequencies with periods from 5 to 20 days.

The average coherence and phase information is presented in Fig. 3 for each of the datasets in this study. For comparison, the results from McNally et al. (1989, Fig. 6) are plotted using the same scales and phase convention. (The computation is done in such a way that a phase of −90° indicates rotating current motion to the right of the rotating wind vector.) It is apparent

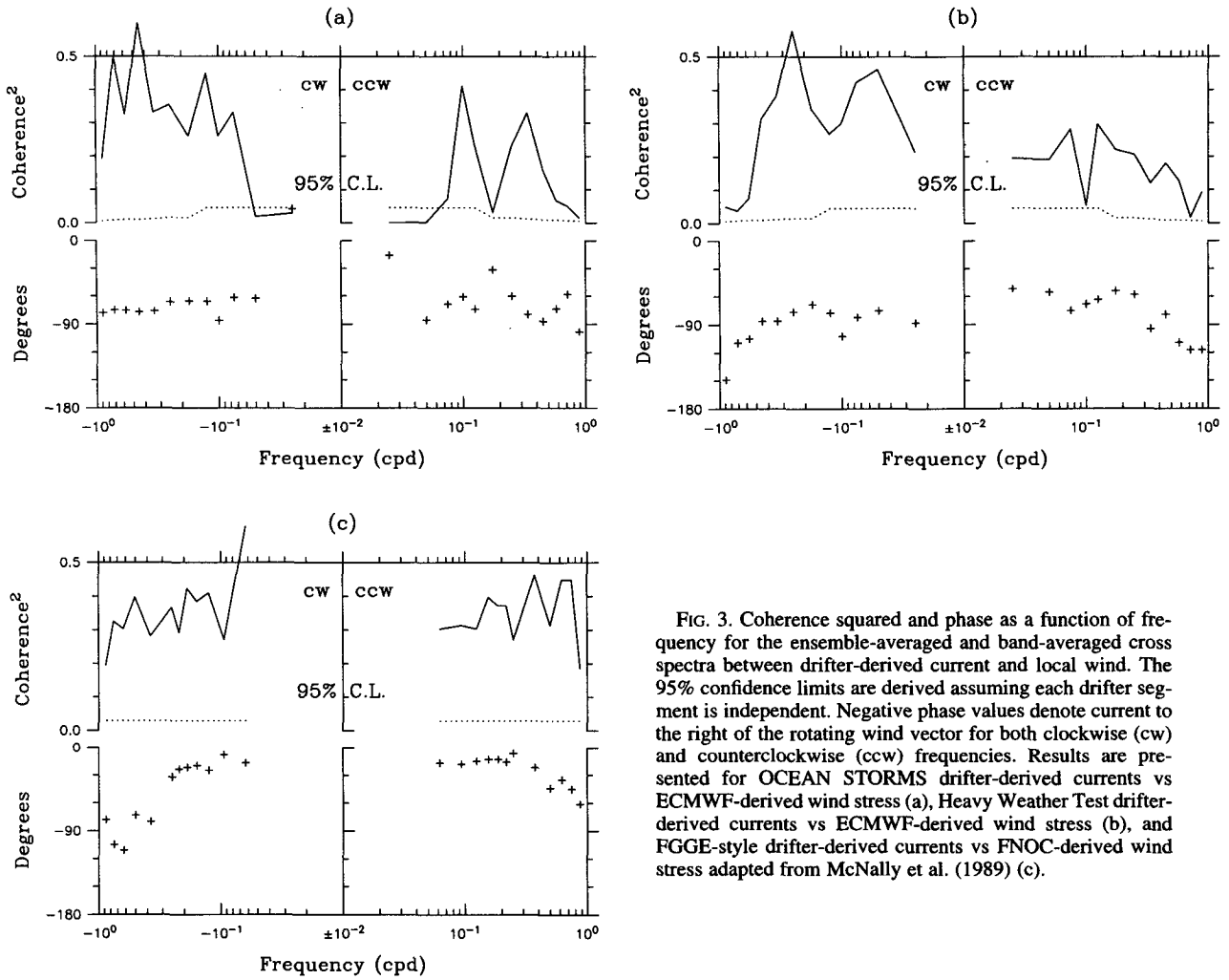

FIG. 3. Coherence squared and phase as a function of frequency for the ensemble-averaged and band-averaged cross spectra between drifter-derived current and local wind. The 95% confidence limits are derived assuming each drifter segment is independent. Negative phase values denote current to the right of the rotating wind vector for both clockwise (cw) and counterclockwise (ccw) frequencies. Results are presented for OCEAN STORMS drifter-derived currents vs ECMWF-derived wind stress (a), Heavy Weather Test drifter-derived currents vs ECMWF-derived wind stress (b), and FGGE-style drifter-derived currents vs FNOC-derived wind stress adapted from McNally et al. (1989) (c).

from Figs. 3a and 3b that, in both analyses, coherences above the 95% confidence level occur for periods between 5 and 20 days. The drop in coherence for periods longer than 20 days is due, we believe, to the presence of mesoscale eddies as sampled by the drifters. Paduan and Niiler (1993) have shown that it takes between 13 and 48 days for drifters in this area to circumscribe mesoscale features with speeds of 10–20 cm s^{-1}. Thus we focus on the 5 to 20 day period band for making a model of the relationship of winds to currents. It is our firm belief that the same model would also apply to the lower-frequency motions except for the fact that the mesoscale eddies introduce a large, incoherent signal into our analysis. The reason for filtering high frequencies out of our simple regression model is that phase is a function of frequency for periods shorter than 5 days. Thus a simple regression model, independent of time lag, would not apply to these motions.

The results in Figs. 3a and 3b show that, for the coherent 5 to 20 day band, the phases are consistently between −60° and −100°, indicating motion to the right of the rotating wind stress vector. These values are close to the phase of −90° expected for currents in a wind-driven mixed layer in which velocity is independent of depth. In these results we have used the full October–April Heavy Weather Test dataset, which extends further into the winter season than does the OCEAN STORMS dataset. The statistical results are similar for either the fall period only or the winter period only, however.

In contrast to the cross-spectral results obtained from our drifter data, the results from the FGGE-type buoys—reproduced in Fig. 3c using our sign convention—show phases consistently greater than −30° (less than 30° to the right of the rotating wind stress vector). The differences in the phase relationship for FGGE-type drifters and our modern drifters is explained by the differences in water-following capabilities between the two classes of instruments. This can be shown using a wind-driven mixed layer model and a model for

downwind slippage as a function of drag area ratio R (see the appendix).

We note that the phase as a function of frequency is quite constant in the 5 to 20 day band. Thus it makes sense to consider linear regression models, which are, in effect, broadband-averaged pictures of the motions. We look at regression results in the next sections in connection with a new model for vertical stress distribution in a wind-driven mixed layer.

b. Regression models

Based on the observation of high coherence and constant phase in the cross-spectral results, we bandpassed filtered all winds, wind stress, and drifter-derived velocities in the period band between 5 and 20 days. A series of regression models were then made based on the following complex vectors: $\mathbf{U} = u + iv$, $\mathbf{W} = W^x + iW^y$, and $\boldsymbol{\tau} = \tau^x + i\tau^y$, where (u, v) are the components of drifter velocity, (W^x, W^y) the components of wind velocity, and (τ^x, τ^y) the components of stress in the x and y directions, respectively.

The first regression that we present is between the drifter and wind velocity and is of the form

$$\mathbf{U} = a\mathbf{W}, \tag{3.1}$$

where the complex number a is determined by a least squares fit over the entire current and wind dataset after currents were corrected for downwind slip and all time series were bandpass filtered in the 5 to 20 day band. The ensemble-averaged regression for the 1987 data gives $|a| = 4.8 \times 10^{-3}$ and direction $-a = -61°$. This regression accounts for 20% of the variance. The ensemble-averaged regression for the 1989/90 data gives $|a| = 5.3 \times 10^{-3}$ and direction $-a = -76°$. This regression, which assumes that all of the motions in the 5 to 20 day band are wind driven, accounts for 34% of the variance. The regressions describe the average state of the time-dependent drifter velocities. For comparison with previous studies, the results suggest that wind-driven currents at 15-m depth can be estimated as 0.5% of wind speed and about 68° to the right of the wind direction (based on the average of regression results for the 1987 and 1989/90 data). Of course, such a rule of thumb result deriving from a steady-state or low-frequency model is of limited usefulness given instantaneous wind observations.

The second regression model is between drifter velocity and wind stress:

$$\mathbf{U} = b\boldsymbol{\tau}_0, \tag{3.2}$$

where τ_0 is the wind stress at the ocean surface. In this case, the ensemble-averaged regression for the 1987 data gives $|b| = 0.25$ m s^{-1}/Pa and direction $-b = -62°$. The ensemble-averaged regression for the 1989 data gives $|b| = 0.28$ m s^{-1}/Pa and direction $-b = -77°$. This regression model accounts for 20% of the variance in drifter velocities in 1987 and 35% of the variance in 1989/90. The model (3.2) and the particular results obtained for these datasets can be coupled with various simple models to develop approximations of stress through an upper-ocean mixed layer that represent improvements over the most commonly used slab-layer profile.

c. Stress models for an ocean mixed layer

The physical models we envisage for the upper ocean are based on the Ekman balance:

$$if\mathbf{U} = \frac{1}{\rho}\frac{\partial \tau}{\partial z}. \tag{3.3}$$

If the stress divergence in the upper ocean were constant, the results of the regression model (3.2) and the Ekman model imply a complex-valued mixing depth,

$$h = \frac{1}{i\rho f b}.$$

The regression model yields $|h| = 37.4$ m and direction $-h = -28°$ for the 1987 data and $|h| = 33.7$ m and direction $-h = -13°$ for the 1989 data. [We do not provide confidence limits on h. The fact that 20%–35% of the variance is explained by the regression model (3.2) is a statement that there is a lot of geostrophic noise and that those limits can be expected to be large.]

The apparent mixing depth scale $|h|$ is smaller than the observed mixed layer depth of, approximately, $H = 60$ m in the OCEAN STORMS area during the fall period (Tabata et al. 1988), which implies that our basal assumption of constant stress divergence over the mixed layer cannot be correct. If the turbulent stress is to vanish at the mixed layer base, the rate of change of turbulent stress with depth would have to be less below the drogue depth than it is at the drogue depth of $h_0 = 15$ m. This result shows that the commonly used slab-layer approximation of a linear stress profile within the mixed layer is not appropriate. Our observations can be used to constrain higher-order stress profiles. We note, however, that this is still an underdetermined inverse problem given our observations at one depth. Many assumed forms of stress as a function of depth could be fit to our observations.

We present two possible models for the distribution of stress in an upper-ocean mixed layer based on simple quadratic and exponential functions. This is useful in order to highlight the differences between these distributions and the commonly used linear distribution. Although we believe these formulations represent improvements over the linear formulation, differences between them show that some aspects of the results are still sensitive to the assumed form of stress profile. We propose the quadratic formulation:

$$\boldsymbol{\tau} = \boldsymbol{\tau}_0 + \alpha z + \beta z^2, \tag{3.4}$$

where α and β are complex constants. Using the formulation (3.4) and the Ekman balance (3.3), these constants can be determined assuming the following constraints at the drogue depth and the mixed layer base:

$$\mathbf{U}(z = -h_0) = \frac{\tau_0}{i\rho f h}, \tag{3.5}$$

$$\tau(z = -H) = 0. \tag{3.6}$$

Evaluation of α and β gives the following upper-layer stress:

$$\tau = \tau_0\left[1 + \frac{z}{H} + \left(\frac{1}{h} - \frac{1}{H}\right)\frac{(H + z)z}{(H - 2h_0)}\right]. \tag{3.7}$$

This result, when combined with the Ekman balance (3.3), yields upper-layer currents of the form

$$\mathbf{U} = \frac{\tau_0}{i\rho f}\left[\frac{1}{H} + \left(\frac{1}{h} - \frac{1}{H}\right)\frac{(H + 2z)}{(H - 2h_0)}\right]. \tag{3.8}$$

The model mixed layer stress and currents in Eqs. (3.7) and (3.8), respectively, contain some familiar properties, such as rotation of the current vector with depth and net transport at 90° to the right of the wind stress vector. Other properties, such as constant velocity shear, are less familiar, particularly when compared with typical slab-layer approximations. The details of these model solutions depend on the ratios of the various observed depth scales, that is, total mixed layer depth, $H = 60$ m, drogue depth, $h_0 = 15$ m, and the apparent mixing depth, $|h| = 34$ m to 37 m, and on the rotation of h, which is obtained from results of the regression model (3.2). Note that, if h is real and equal to the mixed layer depth H, the model simplifies to the commonly used slab-layer approximation.

In order to provide a measure of the sensitivity of these results to the shape of the stress profile, we propose the alternative exponential formulation:

$$\tau = \tau_0 + \gamma(e^{\lambda z} - 1), \tag{3.9}$$

where γ and λ are complex constants. These constants can also be evaluated under the constraints (3.5) and (3.6), although an explicit solution in terms of the depth scales is not available. The mixed layer condition (3.6) requires $\gamma = -\tau_0/(e^{-\lambda H} - 1)$. Constraints at the drogue depth require that

$$\frac{1}{h} = \frac{-\lambda e^{-\lambda h_0}}{(e^{-\lambda H} - 1)}, \tag{3.10}$$

which can be solved iteratively for λ given a particular set of depth scales. For the scales in our observations, we find $\lambda = (0.060, 0.036)$ m^{-1}.

The distributions of the model mixed layer stresses and currents are presented in Fig. 4 for an eastward wind stress, $\tau_0 = (1.0, 0.0)$ Pa, and the average regression parameter $\mathbf{b}$. Results are presented for both the quadratic and exponential stress formulations. In each case, the downwind stress is maximum at the surface and decays monotonically toward the mixed layer base. The divergence of this stress drives flow to the right of the wind. The stress component to the left of the wind stress is zero at the surface and at the mixed layer depth and has a middepth minimum. The divergence of this stress drives downwind flow. In the quadratic stress model, the curvature in the stress field is constant with depth and, therefore, the shear of the current is constant. In the exponential case, the current shear is concentrated toward the top of the layer. Interestingly, the downwind current changes sign at middepth in both model mixed layers and the flow at the mixed layer base is predominantly upwind. The current direction is 61° (60°) to the right of the wind vector at the surface and 178° (184°) to the right of the wind vector at the mixed layer base in the solution for the quadratic (exponential) stress formulation. The changing direction of the model current with depth is illustrated in Fig. 5, which shows the hodograph of model currents for both stress formulations. The magnitude of the shear across the mixed layer base is significantly different between the two model simulations. In the quadratic formulation, this shear is similar to that in a slab-layer model but the direction is nearly opposite for the depth scales we observed in the northeast Pacific. In the exponential formulation, the direction of the shear across the mixed layer base is also opposite to the slab-layer model but the magnitude is much reduced.

4. Summary

This study has compared near-surface velocity measurements from a large number of drifters with local wind velocity and stress. The measurements were made in the northeast Pacific Ocean in the fall of 1987 as part of the OCEAN STORMS Experiment and in the fall and winter of 1989/90 as part of the WOCE Heavy Weather Experiment. The drifters used in the study were of a modern TRISTAR or Holey-Sock design. (In this context, modern refers to the fact that the drifters have large drogues and large drag area ratios as well as to the fact that the drifters have been calibrated for downwind slip as a function of wind speed and drag area ratio.) We have been able to resolve the apparent contradiction in the literature in which subinertial period, near-surface currents were found to be nearly 90° to the right of the wind stress direction for moored current meter observations (e.g., Davis et al. 1981) but less than 30° to the right of the wind stress direction for FGGE-style drifter observations in the same region (e.g., McNally et al. 1989). Our results using heavily drogued drifters show subinertial period currents moving at approximately 70° to the right of the wind stress direction. The differences can be accounted for by possible differences in water-following capabilities of the

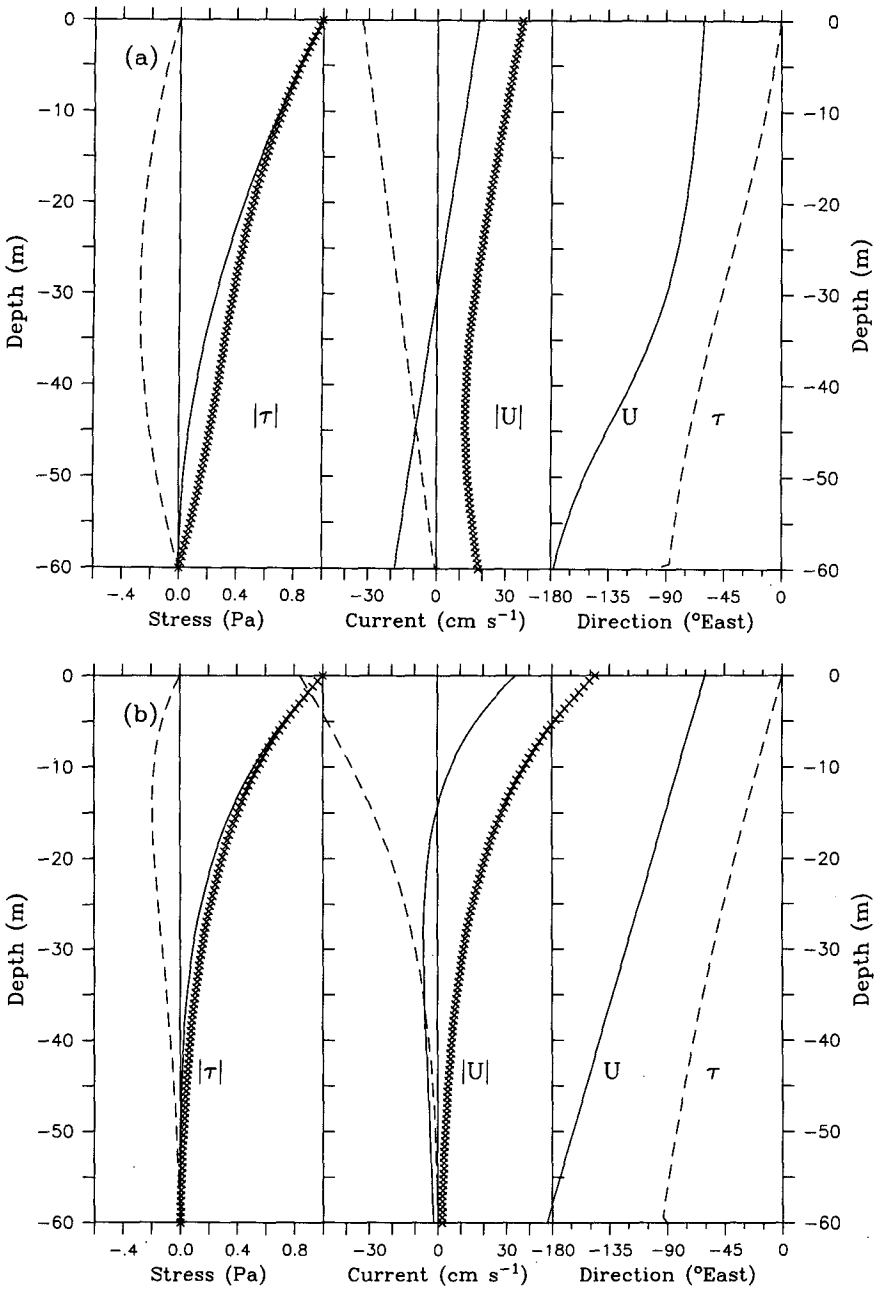

FIG. 4. Model downwind (solid, left panel) and left-of-the-wind (dashed, left panel) turbulent stress components and the turbulent stress magnitude (symbols, left panel) as a function of depth in the mixed layer; model downwind (solid, middle panel) and left-of-the-wind (dashed, middle panel) current components and magnitude (symbols, middle panel) as a function of depth in the mixed layer; model current (solid, right panel) and stress (dashed, right panel) relative to the downwind direction. Results were obtained using a surface wind stress magnitude of 1 Pa and observed values of $H = 60$ m, $h_0 = 15$ m, and $b = (0.09-0.25i)$ m s^{-1}/Pa using the quadratic (a) and exponential (b) stress functions.

different drifter designs: the earlier results from FGGE-style drifters may have been dominated by large downwind slips due to the insufficient drag area ratio of those instruments. By contrast, the modern drifters have drag area ratios up to seven times greater than the FGGE-style drifters and, although they are still not perfect water-following devices, they follow the water motions with much less downwind slip.

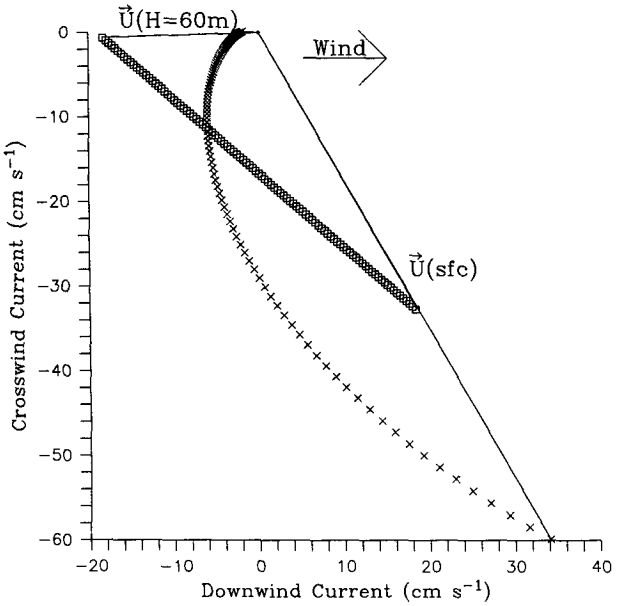

FIG. 5. Hodograph of model currents as a function of depth in the mixed layer. The current direction rotates to the right with depth. Results were obtained using a surface wind stress magnitude of 1 Pa and observed values of H = 60 m, h_0 = 15 m, and b = (0.09–0.25i) m s^{-1}/Pa using the quadratic (squares) and exponential (crosses) stress functions.

Using the calibration data for the modern drifters published by Niiler et al. (1995) and a simple slab-layer model of the upper ocean, it is possible to reproduce the observed phase differences between wind and current vectors as a function of drag area ratio. This is done in the appendix. The model phase results depend on the slab-layer thickness and, to a lesser extent, on the subinertial frequency. For observed ranges of these parameters, the expected phase difference between wind and current vectors are between 60° and 85° for drifters with drag area ratios of 70, such as those used in this study. The same model predicts phase differences of 20°–60° for drifters with drag area ratios of 10, such as the FGGE-type drifters. In all cases, the model phase predictions as a function of drag area ratio tend to flatten for ratios above 40, which suggests that this may be a reasonable minimum value for future surface drifter designs.

The coherence and phase information obtained for the current and wind vector comparisons showed high coherence and nearly constant phase in the period band between 5 and 20 days. We believe that the same results would also hold for longer periods if it were not for the contamination of the wind-driven statistics by currents associated with mesoscale eddies. Given these results, we formed various regression models using current and wind data that had been bandpass filtered in the 5 to 20 day band. The regression results with vector currents modeled as a complex constant times wind predict averaged currents of about 0.5% of the wind speed directed 60° to the right of the wind vector. This angle is slightly less than the typical phase difference for the cross-spectral analysis because, presumably, the mean results are less able to isolate wind-driven processes.

The measurements of Niiler et al. (1993) at these latitudes show that there are high coherences between local wind stress curl $\nabla \times \tau_0$ and deep currents that can account for current speeds of several centimeters per second. These pressure-gradient-driven currents are about the same magnitude as the presumed wind-driven currents we observed in this study. However, a calculation using deep currents and local wind stress τ_0 shows no significant coherence, which is understandable because wind stress and wind curl are 90° out of phase at these frequencies. [See Niiler et al. (1993) for a review of published results on deep current relationship to wind and wind curl.] We therefore believe that, even though there are pressure-gradient-driven currents related to *distant* winds, there are not significant pressure-gradient-driven currents related to *local* winds in this open-ocean setting. Hence, it is appropriate to attribute the wind-coherent motions we observed to direct wind forcing.

A regression model with vector current equal to a complex constant times wind stress yielded a constant with magnitude 0.27 m s^{-1}/Pa directed 70° to the right of the wind stress vector. If this result is interpreted in the framework of a slab-layer Ekman balance, it implies an apparent mixing depth of 36 m, which is less than the observed mixed layer depth of, approximately, 60 m. This observed discrepancy in depth scales suggests a rotating, nonlinear turbulent stress distribution in the mixed layer. We presented solutions for both quadratic and exponential forms of turbulent stress,

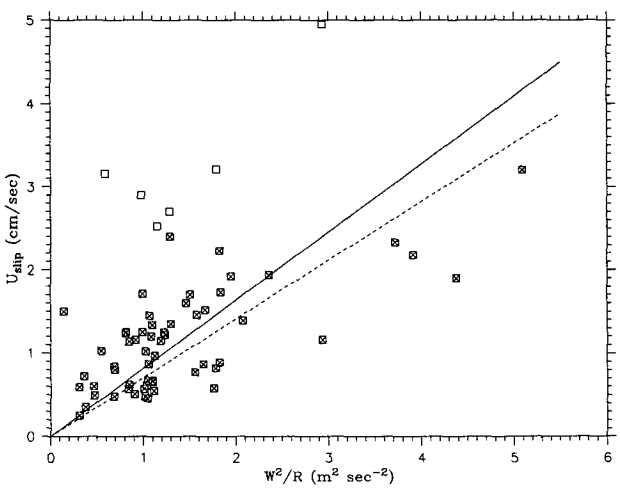

FIG. 6. Observed downwind slip as a function of wind speed squared over drag area ratio from the field measurements of Niiler et al. (1995). Best-fit lines for all observations (solid) and omitting the open symbol outliers (dashed) are also shown.

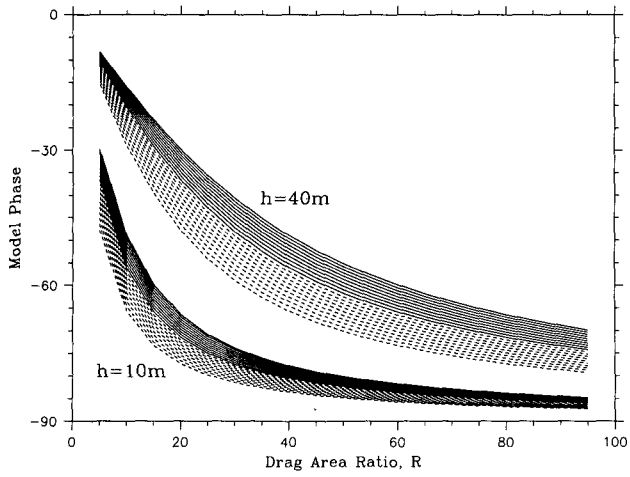

FIG. 7. Predicted phase difference between drifter-derived vector currents and wind stress for a wind-driven slab as a function of drag area ratio. Negative values denote flow to the right of the rotating wind vector. Results are for two values of slab-layer thickness (h = 10 m and h = 40 m) and for periods between 2 and 40 days. Both positive (solid) and negative (dashed) frequencies are shown with results of longer period motions making up the more central traces.

which for the depth scales observed in the northeast Pacific imply current rotations from 60° to the right of the wind stress vector at the surface to 180° to the right of the wind stress vector at the mixed layer base. Cross-wind current magnitudes based on the stress divergence have subsurface maxima in the middle of the mixed layer. This maximum is centered in the mixed layer for the quadratic stress profile but is concentrated nearer the surface in the exponential case. Shear across the mixed layer base is predicted to be of similar magnitude, but opposite direction, to that used in more common, nonrotating slab-layer approximations in the quadratic case. In the exponential case, shear across the mixed layer base is also directed upwind but the magnitude is smaller than that of the nonrotating slab-layer approximation.

Other simple stress models are possible given the depth scales and regression coefficients observable using combined drifter and wind data. The robust result of our measurements is that stress must rotate with depth if it is to vanish at the mixed layer base and still fit with our observations at 15 m. Evidence for rotating stress divergence of the type suggested here is found in the mooring results of Davis et al. (1981). Future analyses of vertically instrumented, upper-ocean current and wind time series may provide insights as to the best shape for models of mixed layer stress distribution. As it is, the models we present may be useful in further correcting drifter-derived current observations. Niiler et al. (1995) provide best-fit slip corrections as a function of wind speed, drag area ratio, and shear across a drifter's drogue element. The stress models presented in this study predict downwind shear on the order of 0.2 cm s^{-1}/m for winds on the order of 10 m s^{-1}. With these parameters, the Niiler et al. (1995) field data shows downwind slips attributable to shear that are fully 80% as large as those slips attributable to wind at the surface. Of course, beyond the goal of enabling more accurate drifter-derived current estimates, the discovery of a more representative model for stress divergence in the upper ocean will benefit all upper-ocean and air–sea interaction models.

Acknowledgments. The authors would like to thank William Large and Greg Crawford for help obtaining the ECMWF wind data and Todd Anderson for assistance verifying ECMWF winds against local observations. Pim van Meurs provided the low-pass filtered drifter data for the Heavy Weather Experiment and Michael Cook helped with many of the calculations. Comments of the anonymous reviewers helped to clarify the presentation of our results. This work was supported by the Office of Naval Research under Contracts N00014-87-K-0005 and N00014-90-J-1153 to the Scripps Institution of Oceanography and Contract N00014-92-WR-24037 to the Naval Postgraduate School.

APPENDIX

Expected Response of a Wind-Driven Slab

The major features of the wind-driven response of surface drifters—including sensitivity to drogue performance—can be exposed with a simple model. In particular, a possible explanation for the differences in downwind slippage between FGGE-type drifters and those used in this study is provided. We begin with the horizontal momentum equation for wind-driven currents:

$$\mathbf{U}_t + if\mathbf{U} = \frac{1}{\rho}\mathbf{T}_z, \qquad \text{(A.1)}$$

where, $\mathbf{U} = u + iv$ and $\mathbf{T} = \tau^x + i\tau^y$ are the complex representations of horizontal velocity and wind stress, respectively. To relate these motions to drifter-derived currents near the ocean surface, note that observed currents are, in general, composed of both wind-driven and non-wind-driven currents. The latter are likely in geostrophic balance, although they are considered as noise to the wind-driven system. There is also error in the measurement of currents from drifter displacement, which has, itself, been measured and modeled.

In general,

$$\mathbf{U}^{\text{obs}} = \mathbf{U} + \mathbf{U}^{\text{slip}} + \mathbf{N}. \qquad \text{(A.2)}$$

Here $\mathbf{U}$ is the wind-driven current that satisfies (A.1), $\mathbf{U}^{\text{slip}}$ is the error in the drifter-derived current, $\mathbf{N}$ is non-wind-driven noise, and each term is a function of time t. The work of Niiler et al. (1995) describes field ob-

servations of $\mathbf{U}^{slip}$ for different drogue configurations under varying wind conditions. They show how the slip past a drogue increases as a function of wind speed and shear across the drogue itself. The slip is also inversely proportional to the drag area ratio R. In most situations, we do not have information about shear but we do have information about winds in the vicinity of the measurements.

A downwind slip model proportional to wind speed over R is capable of explaining 45% of the variance in the Niiler et al. (1995) field data. This model, which does not explicitly account for shear across the drogue, has the following, simple form:

$$|\mathbf{U}^{slip}| = \frac{A}{R}\mathbf{W}. \tag{A.3}$$

For $\mathbf{U}^{slip}$ and $\mathbf{W}$ in m s^{-1}, $A = 0.07$. The direction of the error vector is downwind. In our wind-driven model, it will be convenient to have an error model based on wind stress, not wind speed. Although the correlation of slip and wind stress over R is not presented in Niiler et al. (1995), it can be derived from their data with only a small decrease in the goodness of fit. We use their data to obtain the best fit to the alternate error model:

$$|\mathbf{U}^{slip}| = \frac{B}{R}|\mathbf{W}|^2. \tag{A.4a}$$

Using all of the field data, we derive a best-fit slope of $B = 8.12 \times 10^{-3}$ s m^{-1}, which explains only 8% of the variance. This fit is shown by the solid line in Fig. 6. A better fit is obtained without the anomalous observations of relatively large slip at low $|\mathbf{W}|^2/R$ (denoted by the open symbols in Fig. 6). For that subset, we obtain a best-fit slope of $B = 7.05 \times 10^{-3}$ s m^{-1}, which explains 22% of the variance and is shown by the dashed line on the figure. Wind stress is related to wind speed through a constant drag coefficient: $T = \rho_{air}C_D|\mathbf{W}|\mathbf{W}$. Hence our final error model is

$$|\mathbf{U}^{slip}| = \frac{B'}{R}\mathbf{T}, \tag{A.4b}$$

where B' is 5.90 m^2 s kg^{-1} based on the better of the two fits to the data.

The frequency-dependent coherence between drifter-derived currents and wind stress can be derived by taking the Fourier transform of equation (A.2), which gives

$$\tilde{\mathbf{U}}^{obs} = \tilde{\mathbf{U}} + \frac{B'}{R}\tilde{\mathbf{T}} + \tilde{\mathbf{N}}. \tag{A.5}$$

The tilde symbol is used to denote the Fourier transform, and each of the terms in (A.5) is a function of frequency ω. We employ a slab-layer approximation for the wind-driven currents where h denotes the layer thickness. If $\tilde{\mathbf{U}}(\omega)$ is obtained from the Fourier transform of (A.1) and (A.5) is multiplied by $\tilde{\mathbf{T}}^*$, we obtain the current–wind stress cross-coherence

$$\tilde{\mathbf{U}}^{obs}\tilde{\mathbf{T}}^* = \left[\frac{B'}{R} + \frac{1}{i\rho h(\omega + f)}\right]|\tilde{\mathbf{T}}|^2 + \tilde{\mathbf{N}}\tilde{\mathbf{T}}^*$$
$$= \left[\frac{B'}{R} + \frac{1}{i\rho h(\omega + f)}\right]|\tilde{\mathbf{T}}|^2, \tag{A.6}$$

where the second equation is true if the noise and wind stress are not coherent.

Equation (A.6) can be used to understand the role of the drifter effectiveness (i.e., the drag area ratio R) in the interpretation of current and wind stress observations. The magnitude of the wind stress spectrum acts to scale the magnitude of the current–wind stress coherence but it does not affect the phase information. Phase is controlled by the relative sizes of the slip and inertial terms. For a perfectly water-following drifter, R is infinite and the phase of the coherence between currents and wind stress is −90°, as it is in the idealized case of a wind-driven slab on the rotating Earth. At the other extreme where R is zero, the drogue is completely ineffective and the observed current and wind stress are in phase. This implies downwind motion of the drifter with no regard to the currents.

Although some of the assumptions involved in (A.6), such as the slab-layer approximation, could be criticized, the dependence of the phase on R is robust. Figure 7 shows the phase of $\tilde{\mathbf{U}}^{obs}\tilde{\mathbf{T}}^*$ as a function of R for two choices of slab-layer thickness and for an inertial period of 16 h. The phase solutions are also shown for a range of frequencies for each choice of layer thickness. The innermost curves in both families are for periods of ±40 days and the outermost curves are for periods of ±2 days with positive frequencies denoted by solid lines. Note that in all cases the phase predicted for poorly drogued drifters with $R < 10$ is within 30° of the downwind value. This is consistent with the results from earlier generation drifters such as those described by McNally et al. (1989) if, in fact, the operational value of R for those instruments was low. For the drifters used in this study, R is between 50 and 70 and the predicted phase is between 55° and 85° to the right of the wind vector. This is also consistent with our observations in section 3.

The phase results are not sensitive to the frequency for frequencies less than the inertial frequency. For thicker slab layers, the observed currents are more downwind for all values of R, but in each case the curves tend to flatten for R in the range 30 to 40. This indicates a reduction in performance enhancement with increasing R above these values. (Note that a better performing drifter is one for which the phase approaches the theoretically perfect value of −90°.) This suggests that a natural compromise design between larger or more complicated drifters and smaller, less expensive drifters is obtained at R values around 40.

REFERENCES

Davis, R. E., R. deSzoeke, and P. Niiler, 1981: Variability in the upper ocean during MILE. Part II: Modeling the mixed layer response. *Deep-Sea Res.*, **12,** 1453–1475.

Kirwan, A. D., Jr., G. J. McNally, E. Reyna, and W. J. Merrell Jr., 1978: The near-surface circulation of the eastern north Pacific. *J. Phys. Oceanogr.*, **8,** 937–945.

McNally, G. J., 1981: Satellite-tracked buoy observations of the near-surface flow in the eastern mid-latitude north Pacific. *J. Geophys. Res.*, **86,** 8022–8030.

——, and W. B. White, 1985: Wind driven flow in the mixed layer observed by drifting buoys during autumn–winter in the mid-latitude North Pacific. *J. Phys. Oceanogr.*, **15,** 684–694.

——, D. S. Luther, and W. B. White, 1989: Subinertial frequency response of wind-driven currents in the mixed layer measured by drifting buoys in the midlatitude north Pacific. *J. Phys. Oceanogr.*, **19,** 290–300.

Niiler, P. P., 1986: The observational basis for large-scale circulation of the oceans. *The General Circulation of the Ocean,* H. Abarbenel and W. Young, Eds., Springer-Verlag, 1–54.

——, R. E. Davis, and H. J. White, 1987: Water-following characteristics of a mixed layer drifter. *Deep-Sea Res.*, **34,** 1867–1881.

——, J. Filloux, W. T. Liu, R. M. Samelson, J. D. Paduan, and C. A. Paulson, 1993: Wind forced variability of the deep eastern north Pacific: Observations of seafloor pressure and abyssal currents. *J. Geophys. Res.*, **98,** 22 589–22 602.

——, A. S. Sybrandy, K. Bi, P-M. Poulain, and D. Bitterman, 1995: Measurements of the water-following capability of Holey-sock and TRISTAR drifters. *Deep-Sea Res.*, in press.

Paduan, J. D., and P. P. Niiler, 1993: Structure of velocity and temperature in the northeast Pacific as measured with Lagrangian drifters in fall 1987. *J. Phys. Oceanogr.*, **23,** 585–600.

Pazan, S. L., and C. A. Friehe, 1978: Performance of an air–sea interaction buoy. *J. Appl. Meteor.*, **17,** 1488–1497.

Sybrandy, A. L., and P. P. Niiler, 1991: WOCE/TOGA Lagrangian drifter construction manual. Tech. Rep., University of California, San Diego, SIO Reference 91/6, WOCE Report Number 63, 58 pp.

Tabata, S., L. A. F. Spearing, R. H. Bigham, B. G. Minkley, J. Love, D. Yelland, J. Linguanti, and P. M. Kimber, 1988: STP/hydrographic observations along line *P*, Station *P*, line *R*, and associated lines in the "OCEAN STORMS" Area: Cruise I: 22 Sept.–16 Oct. 1987, Cruise III: 24 Nov.–9 Dec. 1987, Canadian Data Report of Hydrography and Ocean Science, 70 pp.